

EUV (13.5nm) Light Generation Using a Dense Plasma Focus Device

William Partlo^a, Igor Fomenkov^a, Daniel Birx^b

^aCymer Inc., 16750 Via Del Campo Court, San Diego, CA 92127

^bApplied Pulse Power Technologies Inc., 3300 Crismore Lane, Oakley, CA 94561

ABSTRACT

A Dense Plasma Focus (DPF) device has been investigated as a source for EUV lithography. Initial characterizations have been made of a prototype DPF employing an all-solid-state pulse power drive. Using the results from a vacuum grating spectrometer combined with measurements with a silicon photo diode, it has been found that substantial amounts of radiation within the reflectance band of Mo/Si mirrors can be generated using the 13.5nm emission line of doubly ionized Lithium. This prototype DPF converts 25J of stored electrical energy per pulse into approximately 0.76J of in-band 13.5nm radiation emitted into 4π steradians. The pulse repetition rate performance of this device has been investigated up to its DC power supply limit of 200Hz. No significant reduction in EUV output was found up to this repetition rate. At 200Hz, the measured pulse-to-pulse energy stability was $\sigma=6\%$ and no drop out pulses were observed. The electrical circuit and operation of this prototype DPF device is presented along with a description of several future modifications intended to improve stability and efficiency.

Keywords: EUV Lithography, Dense Plasma Focus, Solid State Pulse Power, Lithium Emission

1. INTRODUCTION

One of several critical technologies required for practical implementation of EUV lithography is a reliable, high brightness EUV light source with emission characteristics well matched to the reflection band of the Mo/Si or Mo/Be mirror systems. Since the proposed all-reflective EUV lithography tools are slit scanning based systems, such an EUV light source must also exhibit high repetition rate capability. In addition to these requirements, a practical EUV light source must operate debris-free or employ an effective debris mitigation strategy.

A Dense Plasma Focus (DPF) device has been investigated as a source for EUV lithography because of its potential for high source brightness and high repetition rate operation. A prototype DPF has been constructed that employs an all-solid-state pulse power drive system. This prototype DPF is based on the development work done toward an efficient electric plasma thruster for space applications¹⁻³.

DPF devices have been investigated as x-ray sources for proximity x-ray lithography⁴⁻⁸. Such investigations found that DPF systems can generate large amounts of radiation suitable for proximity x-ray lithography, but were limited in repetition rate due to large per pulse electrical energy requirements, and short lived internal components. The stored electrical energy requirements for these systems ranged from 1kJ to 100kJ. The repetition rates did not exceed a few pulses per second.

If the desired photon energy is reduced from the 1keV level required for proximity x-ray lithography down to 100eV, a scaled-down DPF device might be constructed that achieves the desired EUV spectral power while consuming only moderate electrical power and operating at a high pulse repetition rate. In addition, advances in all-solid-state pulse power technologies have made reliable multi-kilohertz electrical drive circuits a practical reality⁹⁻¹¹.

2. DENSE PLASMA FOCUS SYSTEM DESCRIPTION

A DPF device consists of coaxial electrodes driven to a voltage potential difference that results in the formation of a conductive plasma sheath between the inner and outer electrodes. Previously, typical DPF systems operated in the range of

10-50kV between electrodes resulting in large stored energies in the drive capacitor. By employing magnetic pulse compression along with careful design of the drive inductance, this prototype DPF can operate below 1kV.

Fig 1 shows a simplified diagram of the electrical drive circuit. The initial storage capacitor, C_0 , is charged on command by the DC power supply. Once full charge is reached, the IGBTs are triggered into conduction causing resonant transfer of energy from C_0 to C_1 . In this prototype system, both capacitor values are equal at 65 μ F. Once peak voltage on C_1 is nearly reached, a set of hollow cathode pre-ionization sources (not shown in Fig 1) are energized to initiate avalanche break down in the gas between the inner and outer electrodes. The saturable reactor placed between C_1 and the central electrode, in this case the anode, provides a momentary hold-off of current flow from C_1 until a uniform plasma sheath has formed at the base of the electrode set.

The low saturated inductance of this drive circuit ensures a rapid rise in current flow and the application of nearly all of the C_1 voltage across the electrode set. Previously reported DPF systems made use of spark gaps or thyratrons with no magnetic pulse compression and thus suffered from much higher drive inductance. For this reason, higher voltage operation was required with these systems.

Once significant current begins to flow through the plasma sheath, $\mathbf{J} \times \mathbf{B}$ forces accelerate the plasma away from the base of the electrode set and toward the end of the anode. The flow of electrons and ions as well as the magnetic field and resulting force vector are shown in Fig 2. Simultaneous with the acceleration of the plasma, the current flowing from C_1 through the series combination of the drive inductance and electrode inductance rises toward a maximum. The plasma sheath is eventually driven off the end of the anode resulting in magnetic forces that compress the gas in this region toward the central axis as shown in Fig 3. During this time, a fraction of the magnetic energy stored in the circuit inductance is transferred to the small region of compressed gas near the tip of the anode. Compression and heating raises the temperature of the ions in this region to levels sufficient for intense emission in the EUV spectral region.

A cross-sectional drawing of the prototype DPF device is shown in Fig 4. The C_0 and C_1 capacitors are each made up of 650 individual capacitors of 0.1 μ F with a 1400V rating. The use of such a large number of parallel capacitors reduces the inductance and equivalent series resistance of the capacitor decks to levels appropriate for matching to the plasma resistance. The IGBTs used to transfer the energy stored in C_0 to C_1 are the same as those used in the all-solid-state pulse power system currently employed in Cymer's excimer lasers. The eight IGBTs used in parallel each have a 1400V rating with an average current handling capability of 1000A.

The inductor and diode shown in Fig 1 near the DC power supply are intended for energy recovery. If there is reflected energy due to overshoot of the C_1 waveshape, the resulting negative voltage on C_0 is converted to positive voltage via a half cycle of LC ringing through this inductor and diode¹². Once this voltage conversion is complete, the recovered energy is available for use in the next pulse.

3. SPECTRAL MEASUREMENTS

Since the Mo/Si mirror systems exhibit high reflectivity only over a narrow band of wavelengths, detailed measurements of the emission spectrum from this prototype DPF are needed to quantify the useable radiation. An Acton Research Corp. Model GIMS-551.5 grazing incidence spectrograph was used for this purpose. This unit employs a curved 1200 groove/mm grating with a 1.5m radius of curvature. The entrance slit is fixed at an incident angle of nominally 88° relative to the grating normal. The exit slit and detector travel on a precision rail along the path of the Rowland circle formed by the curved grating. Both the entrance and exit slits are adjustable. An optimum resolution/sensitivity combination was achieved with 50 μ m entrance and exit slits and all measurements shown in this paper were made with this slit width.

The detector placed behind the spectrometer exit slit is a Hamamatsu Corp. model R5250-10 EMT with a BeO first dynode. The quantum efficiency of this EMT is relatively constant over the wavelength range of interest, varying by approximately a factor of 2.5 over the range from 10nm to 24nm. Proper operation of this EMT requires a background pressure of 1mT or less. To achieve low pressure in the EMT region while simultaneously operating the DPF at 100mT or greater, required the use of two turbo-molecular pumps each pumping differentially. One turbo-molecular pump was attached to the volume located between the two spectrometer slits and the second evacuated the region behind the exit slit. This arrangement is

shown in Fig 5 along with the various other diagnostics used in evaluating this prototype DPF. The distance between the DPF and the entrance slit of the spectrometer was 50cm. No relay optics were used between the DPF and the spectrometer.

Initial characterizations were made using a solid Tungsten anode and a buffer of 100mT of Xenon gas. The measured spectrum for these conditions is shown in Fig 6. Also included in this figure is the published transmission through 50cm of Xenon at 100mT. By switching to a different buffer gas, we can determine if the broad spectral feature between 15nm and 30nm is due to emission from Tungsten or Xenon. Fig 7 shows the same measurement but with a buffer of 200mT of Argon. The same broad spectral feature exists with minor changes most likely due to the differences in transmission between Xenon and Argon. Note the absorption feature in the Xenon buffered spectrum at 18.5nm. This feature matches well with the published Xenon transmission data¹³.

By placing a small amount of Lithium on the tip of the anode, the emission spectrum can be changed from predominately Tungsten to that of Lithium. Lithium has been proposed as an emission source for EUV lithography because of its narrow spectrum and intense emission into wavelengths well matched to the reflectance band of Mo/Si mirrors¹⁴. Fig 8 shows the measured emission spectrum of the DPF Lithium plasma over a range from 10nm to 24nm. This measurement was made with 200mT of Argon Buffer gas.

The Lithium emission lines between 10nm and 14nm are due to electronic transitions of doubly ionized Lithium, also referred to as Hydrogen-like Lithium. Verifying the wavelength calibration of the spectrometer is simplified by the fact that the Hydrogen-like Lithium lines are narrow and well known. Using this experimental setup, we can locate six electronic transitions of doubly ionized Lithium as shown in Fig 9. After making a fit to these six spectral lines, it is found that the entrance angle of the spectrometer is 87.5° relative to the grating normal. Using this entrance angle and the grooves/mm of the grating one can generate a conversion factor between wavelength and position along the Rowland circle.

As shown in Fig 8, the 13.5nm Lithium emission line matches well to the Mo/Si reflectance band. A finer resolution spectral scan centered on 13.5nm is shown in Fig 10 along with the published reflectivity of a Mo/Si mirror. The measured bandwidth for this 13.5nm emission line is 0.03nm. It is suspected that this result may be spectrometer resolution limited and the bandwidth of this emission line is likely less than 0.03nm. Fortunately, the exact bandwidth of this emission line is unimportant to the operation of the Mo/Si mirror since even the measured 0.03nm result is much more narrow than the reflectance bandwidth of the Mo/Si mirror.

4. 13.5nm ENERGY MEASUREMENTS

Calorimeters, vacuum photodiodes, and silicon photodiodes are three types of detectors typically used for making absolute energy measurements in the EUV wavelength region. A silicon photodiode was used to characterize the in-band energy per pulse generated by this prototype DPF.

Silicon based photodiodes with EUV transmitting passivation layers are now routinely available. The photodiode used for these measurements was fabricated by International Radiation Detectors, model No. AXUV-100^{15,16}. This photodiode possesses a 60Å thick passivation layer of silicon dioxide with negligible absorption. In the wavelength region of interest, these photodiodes exhibit a quantum efficiency given by (photon energy)/3.63eV. For the radiation centered at 13.5nm, the quantum efficiency is 25.2.

Two methods of filtering the incident radiation were investigated. The first attempt was to make use of a free standing filter placed in front of a bare AXUV-100 photodiode. This filter consisted of Yttrium and Silicon layers with 3500Å and 2500Å thickness respectively. Even with a silicon wire mesh, these filters were found to be too fragile for practical use. The second attempt at filtering was to purchase special versions of the AXUV-100 photodiode with a Ti/Y/C coating placed directly on the photodiode. The thickness of these layers is 60Å/2000Å/500Å respectively.

Since the transmission of the Ti/Y/C filter encompasses more than the 13.5nm Lithium emission line, the measured Lithium emission spectrum must be used to properly partition the photodiode signal according to the various emission lines. Starting with the measured EMT signal vs. wavelength for Lithium as shown in Fig 8, we must compensate for the wavelength dependence of the following: EMT quantum efficiency, grating reflection efficiency, Argon transmission between DPF and spectrometer entrance slit (50cm), Argon transmission between DPF and filtered photodiode (70cm), photodiode filter transmission, and photodiode quantum efficiency. The only factor in this list that is not known is the grating reflection

efficiency. For these measurements, the grating reflectivity is assumed to be constant between 10nm and 24nm. The rest of these factors are shown in Fig 11. Combining these factors with the measured Lithium plasma emission of Fig 8 gives the result that 69% of the charge generated by the photodiode is due to the 13.5nm emission line.

The Ti/Y/C filter is also highly transmitting to hard x-rays. If this prototype DPF produces any hard x-ray photons, they will be heavily weighted by the photodiode because of the diode's high quantum efficiency for high energy photons. An uncoated AXUV-100 photodiode located behind a 25 μ m thick Beryllium foil generated no signal when the DPF was operated with Lithium, thus demonstrating that no hard x-rays are produced under these conditions. However, a measurable amount of hard x-rays can be detected through the Beryllium foil when the DPF is operated with Tungsten and a low buffer gas pressure (50mT).

Using the filtered photodiode, the calibrated in-band 13.5nm energy radiated from the DPF is 0.76J per pulse into 4π steradians. For this measurement the electrical energy initially stored on the C_1 was 25J per pulse. Thus, the 13.5nm radiation represents 3% of the total electrical energy applied to the DPF.

5. REPETITION RATE SCALING

The proposed all-reflective EUV lithography tools are slit scanning based systems. Because of the sliding window nature of the scanning exposure, any practical EUV light source must be capable of high repetition rate operation. Even with perfect pulse-to-pulse energy stability, a minimum of 10-20 pulses per sub-field are required to eliminate the dose errors associated with a pulsed exposure source and a continuously scanning exposure field. If the stability of the exposure source is less than perfect, then the necessary number of pulses per sub-field further increases.

State-of-the-art wafer stage scanning speeds are approaching 250mm/s. The slit width of all-reflective EUV projection optical systems is expected to be smaller than corresponding DUV scanning systems. For example, the EUV LLC Engineering Test Stand has a designed slit width of 1.5mm as compared to the 5-8mm slit widths used on DUV scanning systems. To achieve a minimum 10 pulse exposure within each 1.5mm sub-field with a stage speed of 250mm, the source repetition rate must be 1,667Hz.

One promising feature of this DPF device is its proven high repetition rate capability when used as an electric plasma thruster for space applications¹⁻³. As a plasma thruster, short bursts of 3,000Hz operation are routinely demonstrated. To investigate the repetition rate capability of this prototype DPF, the repetition rate was increased for short bursts while monitoring the EUV radiation output. Up to the DC power supply limited repetition rate of 200Hz there was no decrease in average EUV output. Fig 12 shows the measured EUV output for a 0.25sec burst at 200Hz. This burst represents an average EUV output of 152W radiated into 4π steradians.

There was no significant burst transient found during these repetition rate measurements and no drop out pulses were observed. The pulse-to-pulse energy stability for the burst shown in Fig 12 is $\sigma=6\%$. Improvements in energy stability beyond this present performance will be required to meet the needs of high throughput EUV lithography tools. In addition to the energy stability, the position stability of the DPF must be characterized and meet a minimum set of requirements for a practical system.

6. FUTURE IMPROVEMENTS

The short burst repetition rate results of this prototype DPF in combination with the successful multi-kilohertz operation of plasma thrusters of similar design lead us to believe that 1000Hz+ operation of this DPF device as an EUV radiation source is possible. Continuous, high average power operation will be limited mainly by thermal loading on the central electrode.

It has been found that the capacitance value used in this prototype DPF is larger than optimum. Evidence of this is shown in Fig 13. The measured voltage and current waveshapes for C_1 are shown along with the 13.5nm radiation intensity. As described in section 1, once avalanche breakdown occurs, the discharge current rapidly rises simultaneous with acceleration of the plasma sheath toward the end of the anode. The DPF occurs once the plasma sheath reaches the end of the anode. After the magnetically stored energy is applied to the DPF (at $t=-0.6\mu$ s in Fig 13), the energy remaining in C_1 contributes

mainly to electrode erosion and heating and very little to 13.5nm output. From the waveshapes shown in Fig 13, we can estimate that approximately 19J of the initial 25J stored on C_1 has yet to leave C_1 at the moment of DPF formation. This remaining 19J does eventually flow from C_1 into the DPF device as seen by the nearly critically damped voltage waveshape in Fig 13. Only 0.081J of energy is recovered during the C_1 voltage overshoot. The rest of the 25J initially stored in C_1 is expended in the electrode region. An optimized (smaller) value of C_1 would lead to less energy remaining on C_1 after the termination of the DPF.

A second method of preventing excess energy deposition into the electrode region would be to implement a shunt element fabricated with saturable magnetics timed to short C_1 to ground just after the DPF terminates. Such a shunt would redirect the remaining C_1 energy away from the electrode region causing the C_1 voltage waveshape to ring negative allowing the pulse-power system to recover this energy for use in the next pulse.

Under expected operating conditions, the DPF device will continuously produce vaporized Lithium. Deposition of Lithium atoms onto Mo/Si mirrors is expected to rapidly degrade mirror performance. A practical EUV lithography source based on the Lithium DPF concept must employ a collector that is tolerant to Lithium deposition.

Nested parabolic reflectors operating at grazing incidence represent a collection scheme that might be made tolerant to Lithium deposition. A prototype optic of this type has been ordered from Parallax Research Inc. This optic consists of 5 nested paraboloids each with a Palladium coating on a Nickel substrate. The optical design for this prototype is intended to collect and collimate a solid angle of 0.38 steradians. If 0.79J of 13.5nm radiation is emitted into 4π steradians, this prototype optic will collect 23mj of in-band radiation per pulse. At a pulse repetition rate of 200Hz, an average in-band power of 4.6W would be collected.

Since this prototype optic is constructed entirely of high temperature materials, it will be possible to raise its temperature above the 180°C melting point of Lithium without damage or reduction in performance. It is expected that operating this optic at elevated temperature will continuously boil off the deposited Lithium from the reflecting surfaces. Surface finish degradation due to Lithium impact is of concern. The working distance for this optic is 4.5cm while the mean free path of Lithium in 200mT of Argon is approximately 0.4mm so the Lithium atoms are expected to have no more than average thermal velocities upon contact with the optic's reflecting surfaces.

7. CONCLUSIONS

Initial characterizations of this prototype DPF have shown that it can produce lithographically significant amounts of radiation with a spectrum well matched to the Mo/Si EUV mirror systems. The demonstrated 200Hz repetition rate exceeds that of most other prototype EUV light sources. Based on experience with this technology in electric plasma thrusters, we expect that multi-kilohertz operation is feasible. The demonstrated system efficiency of 3% is competitive with other source technologies and should further improve with the changes planned for this prototype machine.

The system geometry allows up to a 2π steradian collection solid angle. An optic based on grazing incidence parabolic reflectors is under investigation as a collection scheme tolerant to Lithium vapor deposition. The relatively high EUV transmission of the Argon buffer gas (91% through 10cm at 200mT) allows consideration of other debris mitigation methods such as foil traps¹⁷.

Position stability of the DPF has yet to be carefully characterized. Initial results show that improvements in pulse-to-pulse position stability will be necessary to take full advantage of the 100-300 μ m source size. Energy stability is likely to be impacted by the same phenomena that effect position stability and thus efforts to improve these performance parameters will be of greatest importance.

ACKNOWLEDGEMENTS

The authors have made extensive use of the EUV transmission data made available by Lawrence Berkeley Labs on their web sight: http://www-cxro.lbl.gov/optical_constants/ and would like to thank those responsible. Guidance and feedback has been provided by Drs. Jeff Bokor and Bill Oldham and we would like to acknowledge their input to this project. We would

also like to thank Kevin Duenow for his tireless efforts in assembly, maintenance, and repair of the equipment used in this research and Ken LaValley for his efforts in designing and detailing many of the components used in this prototype.

REFERENCES

1. J. Ziemer, E. Cubbin, E. Choueiri, and D. Birx, "Performance Characterization of a High Efficiency Gas-Fed Pulsed Plasma Thruster," *33rd AIAA/ASME/SAE/ASEE Joint Propulsion Conference*, Seattle, WA, 1997.
2. J. Ziemer, E. Choueiri, and D. Birx, "Trends in Performance Improvements of a Gas-Fed Pulsed Plasma Thruster," *25th International Electric Propulsion Conference*, Cleveland, OH, 1997.
3. D. Birx, "Plasma Gun and Methods for the use Thereof," *US Patent 5,866,871*, Feb. 2, 1999.
4. D. Nagel, "Plasma Sources for X-ray Lithography," *VLSI Electronics: Microstructure Science*, vol 7, pp 137-170, 1984
5. E. Cullman and T. Kunne, "Comparison of Different X-ray Sources using the same Printing Process Parameters," *J. Vac. Sci. Technol. B*, 5 (3), pp 638-640, May/June, 1987.
6. Y. Kato, et. al., "Plasma Focus X-ray Source for Lithography," *J. Vac. Sci. Technol. B*, 6, (1), Jan/Feb, 1988.
7. A. Heuberger, "X-ray Lithography," *J. Vac. Sci. Technol. B*, 6, (1) Jan/Feb, 1988.
8. J. Eberle, et. al., "Plasma Focus as a Radiation Source for X-ray Lithography," *Microelectronic Engineering*, Vol. 3, pp 611-613, 1985.
9. T. Watson, et. al., "Laser Having Improved Beam Quality and Reduced Operating Cost," *U.S. Patent 5,748,656*, May 5, 1998.
10. D. Knowles, et. al., "Reliable, Modular, Production Quality Narrow Band KrF Excimer Laser," *U.S. Patent Pending*.
11. D. Myers, et. al., "Production-Ready 2kHz KrF Excimer Laser for DUV Lithography," *Proc. SPIE 3679*, March, 1999.
12. D. Birx, et. al., "Pulse Power Generating Circuit with Energy Recovery," *U.S. Patent 5,729,562*, Mar. 17, 1998.
13. J. Blackburn, P. Carroll, J. Costello, and C. O'Sullivan, *J. Opt. Soc. Am.*, Vol 73, pp 1325, 1983.
14. M. Klosner and W. Silfvast, "Feasibility of Various Discharge Configurations for High Intensity Lithium Vapor Discharge Source at 13.5nm for EUVL," *OSA TOPS on Extreme Ultraviolet Lithograph*, Vol. 4, May, 1996.
15. L. Canfield and J. Kerner, "Silicon Photodiodes Optimized for the EUV and Soft X-ray Regions," *SPIE Proc. on X-ray and Gamma-Ray Instru. for Astronomy*, Vol. 1344, pp 372-377, 1990.
16. E. Gullikson, et. al., "Stable Silicon Photodiodes for Absolute Intensity Measurements in the VUV and Soft X-ray Regions," *J. of Elec. Spect. and Related Phenomena*, Vol. 80, pp 313-316, 1996
17. L. Shmaenok, et. al., "Demonstration of a Foil Trap Technique to Eliminate Laser Plasma Atomic Debris and Small Particulates," *SPIE Proc. on Emerging Lithographic Technologies II*, Vol. 3331, pp 90-94, Feb., 1998.

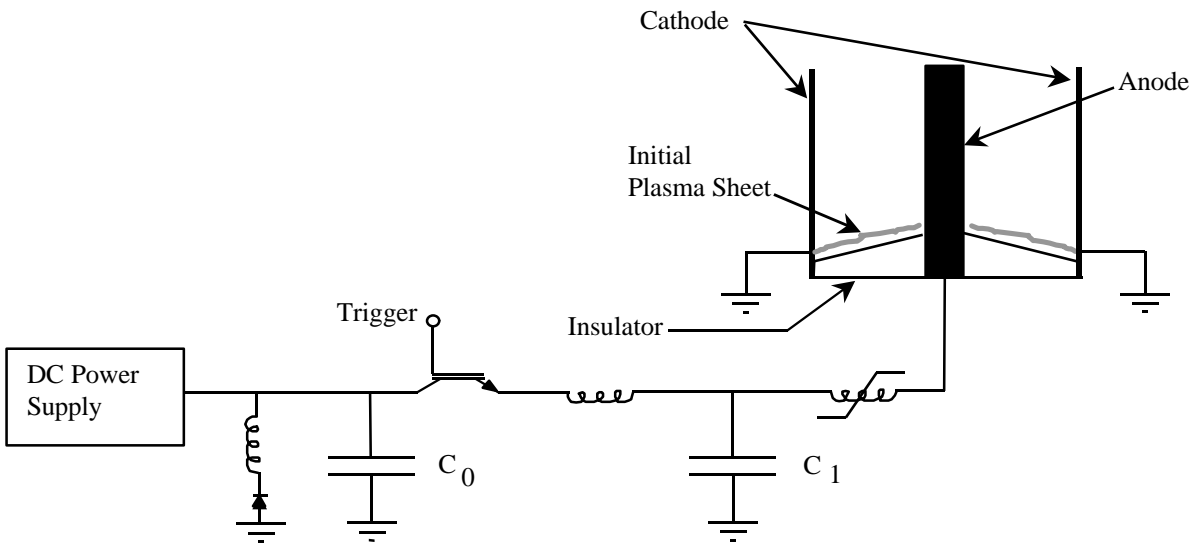


Fig 1 Simplified diagram of electrical drive circuit and DPF electrode set.

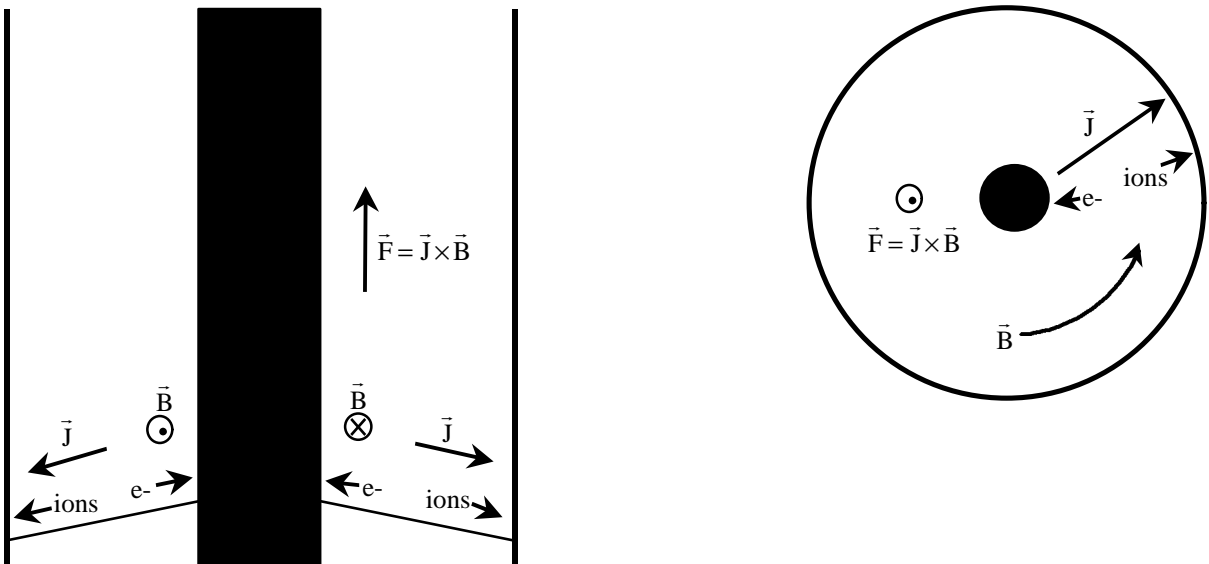


Fig 2. Electron and Ion current flow and resulting force vector in plasma sheath.

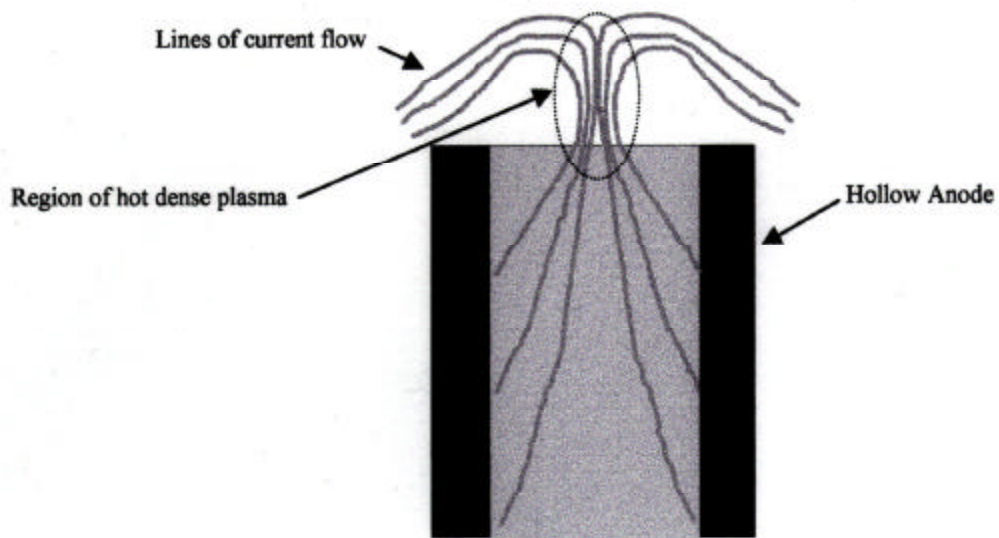


Fig 3. Compression and heating of gas located near tip of anode as plasma sheath accelerates off end of anode.

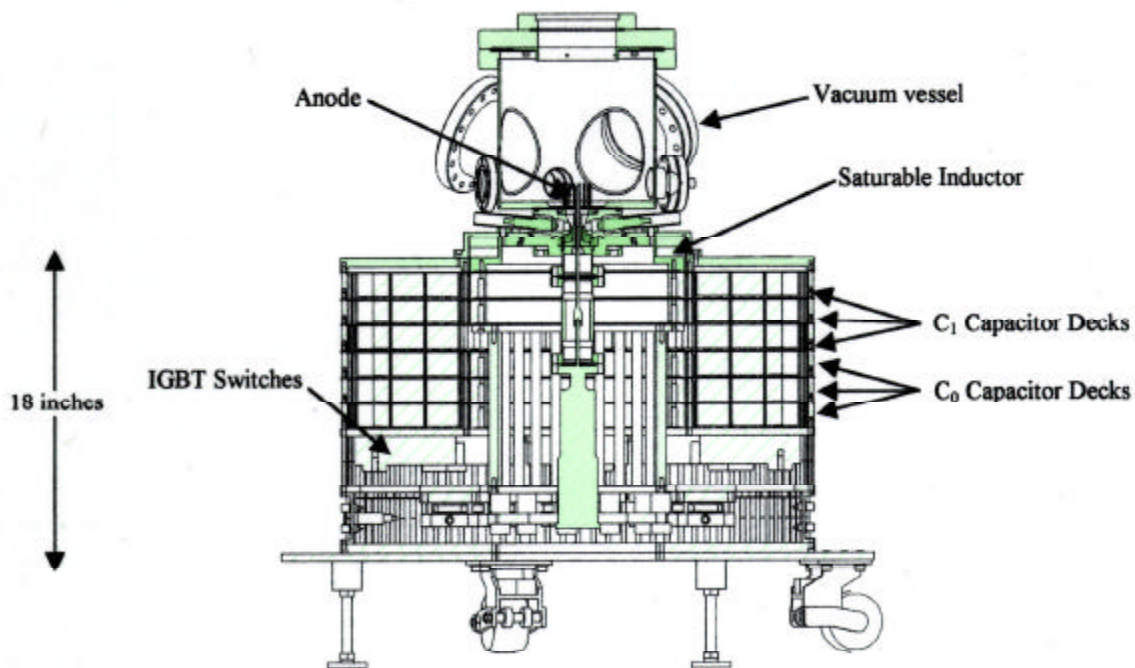


Fig 4. Cross-sectional drawing of prototype DPF device.

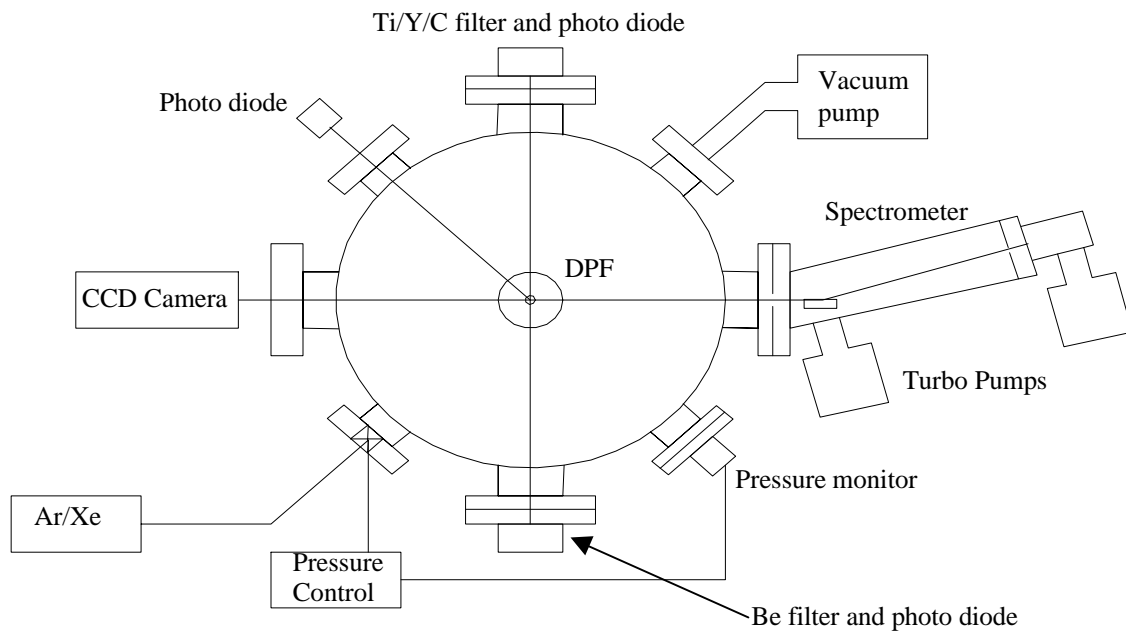


Fig 5. Experimental setup.

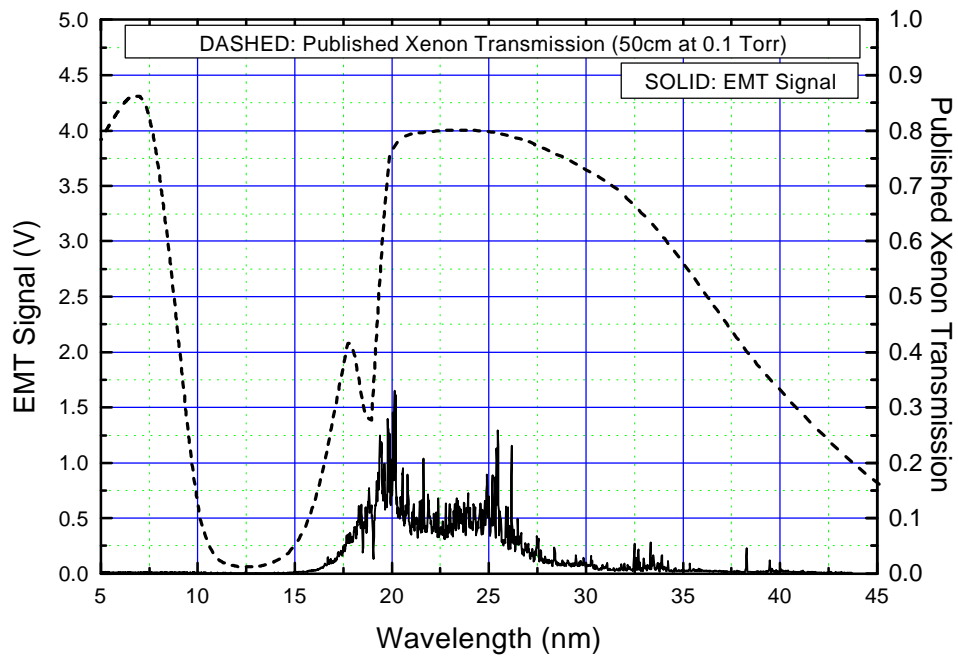


Fig 6. Measured EUV spectrum with solid Tungsten electrode and 100mT of Xenon buffer gas.

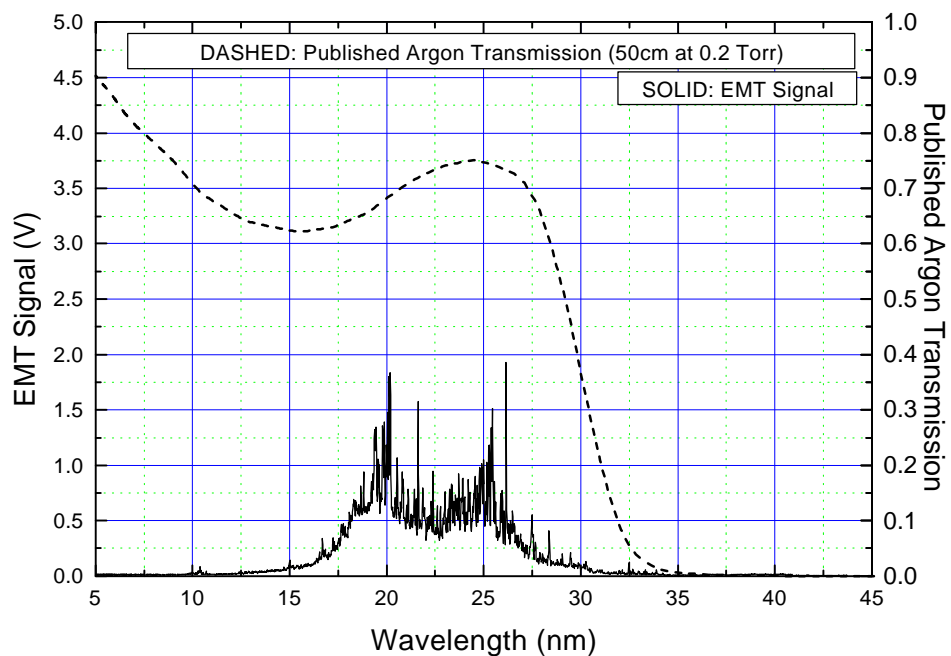


Fig 7. Measured EUV spectrum with solid Tungsten electrode and 200mT of Argon buffer gas.

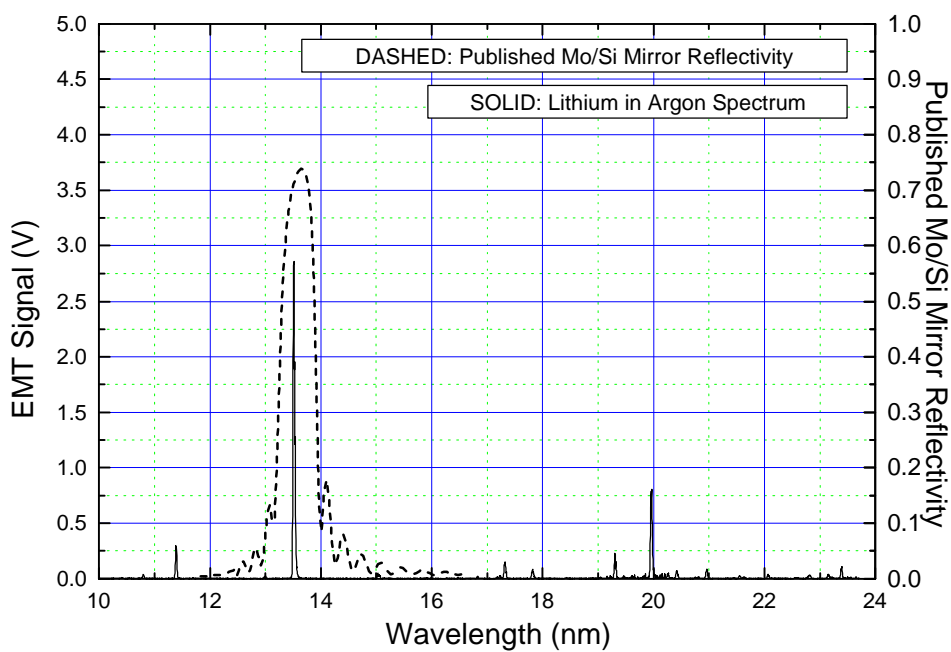


Fig 8. Measured EUV spectrum of Lithium plasma with 200mT of Argon buffer gas.

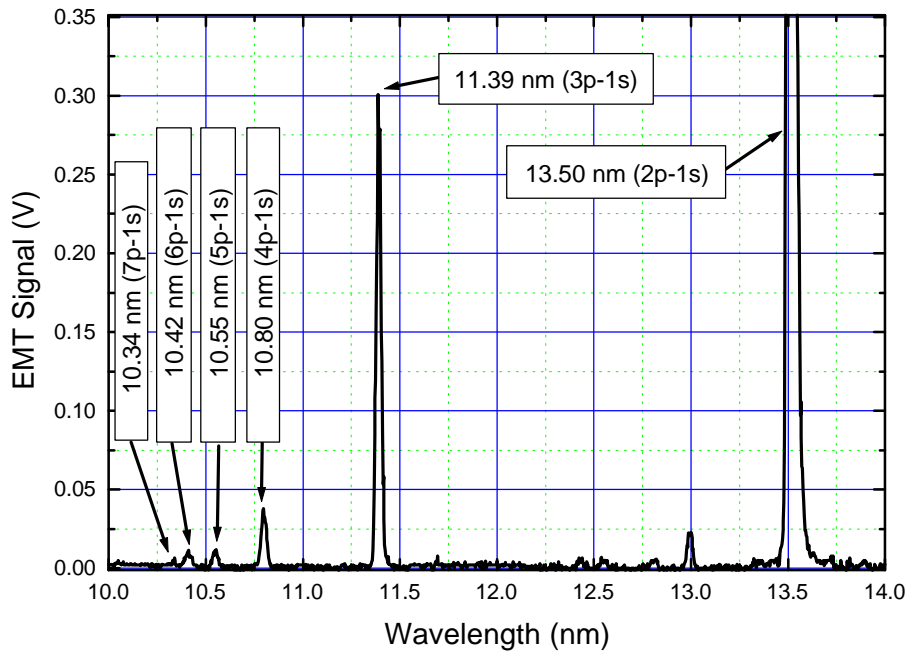


Fig 9. Measured emissions from electronic transitions of doubly ionized Lithium.

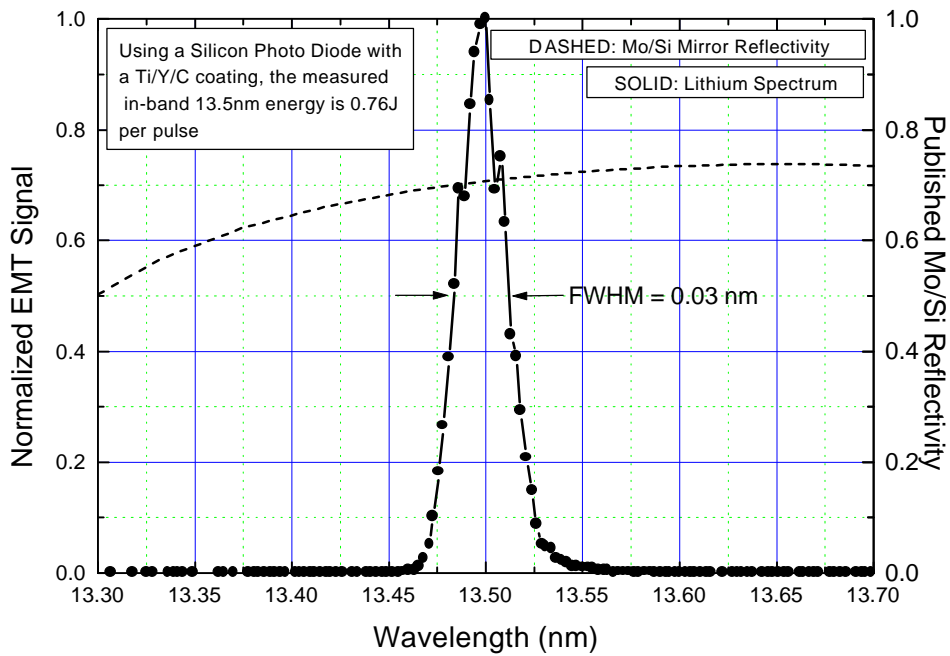


Fig 10. Fine resolution spectral scan of Lithium plasma 13.5nm emission line.

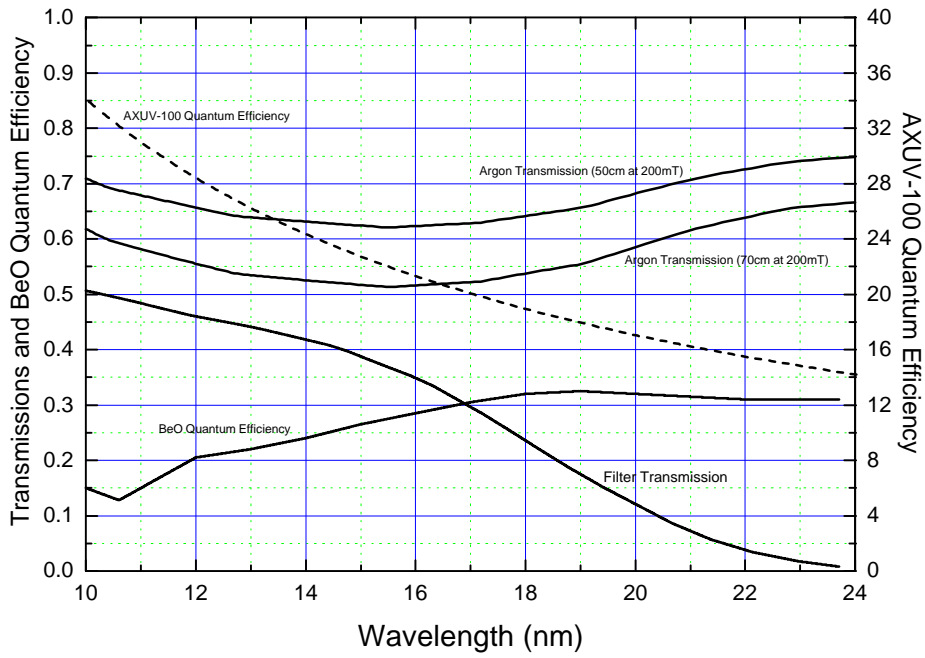


Fig 11. Calibration factors used to determine partitioning of EUV energy in filtered photo diode signal.

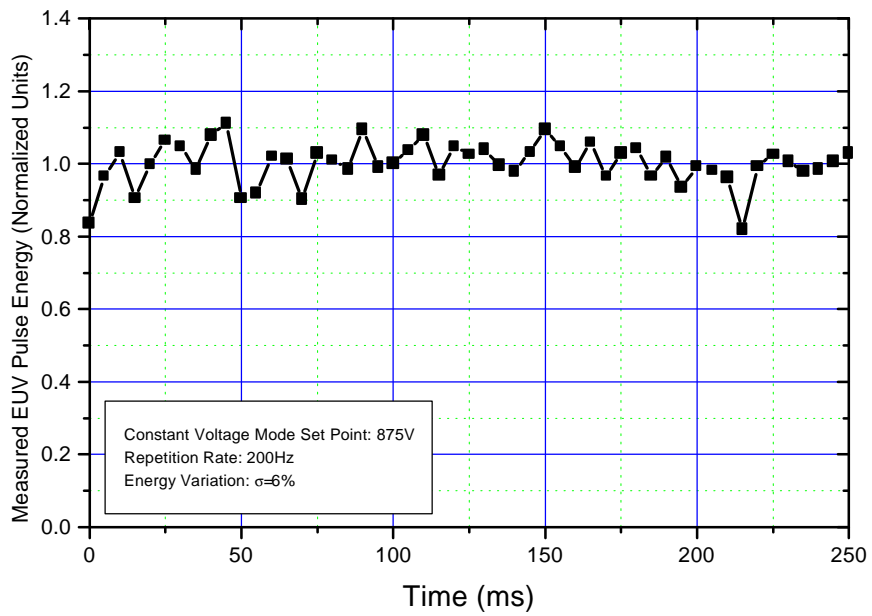


Fig 12. Measured EUV pulse energy for a 0.25sec burst at a PRF of 200Hz.

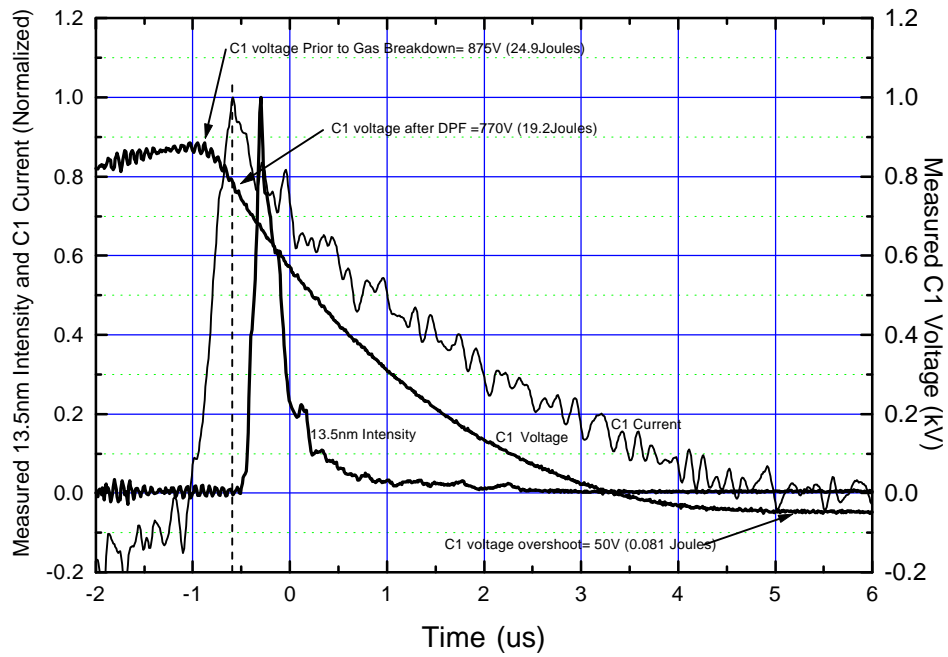


Fig 13. Measured voltage and current waveshapes along with 13.5nm output.